Hindawi
Shock and Vibration
Volume 2024, Article ID 2329389, 18 pages
https://doi.org/10.1155/2024/2329389

Research Article

Dynamic Response of Offshore Wind Turbine with a New Monopile Foundation under Different Lateral and Seismic Loadings

Mehdi Ebadi-Jamkhaneh [1] **and Denise-Penelope N. Kontoni** [2,3]

[1]*Department of Civil Engineering, School of Engineering, Damghan University, Damghan, Iran*
[2]*Department of Civil Engineering, School of Engineering, University of the Peloponnese, GR-26334, Patras, Greece*
[3]*School of Science and Technology, Hellenic Open University, GR-26335, Patras, Greece*

Correspondence should be addressed to Denise-Penelope N. Kontoni; kontoni@uop.gr

Received 16 December 2022; Revised 6 September 2023; Accepted 9 January 2024; Published 30 January 2024

Academic Editor: Chao-Ping Zang

Using a monopile foundation due to a reliable and simple technology has a wide application in engineering structures. This paper investigates numerically the performance of an offshore wind turbine with a monopile foundation equipped with a restriction plate at a middle inside height of the monopile under the wind, wave, and seismic loadings. Different parameters, including wind velocity, wave period, wave height, soil characteristics, and combination of loadings, are considered in nonlinear finite element dynamic analyses. Results are given in terms of the distribution of displacement and bending moment over the turbine height and frequencies. The results reveal that by increasing the wind velocity, the responses of the tower increase, and the wind load acting on the hub has the most important effect on the turbine behavior rather than the wind load acting on the tower body. Furthermore, the values of maximum displacement and bending moment under wind and wave loading decrease with the increase of the shear strength of the soil, whereas the responses of the tower under earthquake loading increase. Generally, it is necessary to consider the effect of a combination of wind, wave, and earthquake loadings on the design of the turbine tower.

1. Introduction

In recent decades, wind-power turbines have become efficient technologies that produce clean electrical energy from the kinetic energy of wind [1, 2]. Wind turbines are typically classified into two types according to their locations: onshore and offshore. Onshore wind turbines are more common than offshore types, but three decades after the first attachment of the offshore wind park in Denmark in 1991, there has been a growing tendency to construct offshore wind farms in the past two decades [3]. Although the onshore type is more easily accessible than offshore wind power, the precise selection of installation location, which ensures sufficient wind speed, the effect on surface air patterns, and its sound pollution, which impacts human health and activity, are challenging problems in onshore wind farms. Due to faster and stronger wind over the water and considering the mentioned challenges, offshore wind farms have been highly regarded in recent years [4–9].

Different kinds of foundations following their location in the ocean are used as a substructure in offshore wind turbines. In depths up to 15 m, monopiles are used due to their simple structure and feasible construction. A combination of the soil-monopile and water-monopile interactions affects the total behavior of the tower under lateral loading.

Many physical models and experiments have been carried out to investigate the interaction between piles and soil without the influence of the superstructure. However, the interaction between structure and foundation must be considered to assess the response of the offshore wind turbine as the soil-pile-tower interaction substantially alters the system's response. To control the constancy of the

flexible offshore wind turbine system, the interaction between the structure and the foundation must be addressed together because the serviceability standards of the monopile at the upper level of the seabed and the tower are different. The current design approach relies mainly on semistatic loading on offshore wind turbines. However, the interaction of soil and structure significantly affects the dynamic behavior of offshore wind turbines. Therefore, it is indeed necessary to carry out a dynamic analysis of offshore wind turbines, taking into account the interactions of soil and structure for the logical design of the structure.

Currently, two methods of modeling soil-structural interactions for dynamic responses of wind turbines are still in use. Using a three-dimensional (3D) solid model and replacing the foundation with linear/nonlinear *p-y* curves are two conventional methods to model offshore wind turbine foundations. Several researchers used the first method to model the offshore wind turbine foundations. An investigation was performed by Kourkoulis et al. [10] to study the behavior of wind turbines resting on caisson foundations and exposed to wave and seismic loadings concerning nonlinear 3D FE methods. The behavior of wind turbines resting on soil under vertical excitation was studied by Kjørlaug and Kaynia [11]. An offshore wind turbine was exposed to wind and wave loading and studied by Corciulo et al. [12] using a dynamic 3D FE analysis. The effect of important parameters (namely, the relative stiffness of structure and soil and the ratio of the layer stiffness to the half-space stiffness) on the behavior of offshore wind turbines was investigated by Taddei et al. [13]. Furthermore, some experimental investigations were performed to study the dynamic response of wind turbines regarding the soil-structure interaction.

According to the Euler–Bernoulli beam-column, an analytical model was developed by Adhikari and Bhattacharya [14]. They considered the foundation as the elastic end support and validated their model by test models. A model based on an analytical transfer matrix method was suggested by Feyzollahzadeh et al. [15] to assess the behavior of offshore wind turbines under wind load. In this method, the foundations are disentangled as coupled springs, distributed springs, and evident fixity length models. A simplified technique for determining the fundamental frequency of wind turbines that are rested on a monopile foundation was proposed by Darvishi-Alamouti et al. [16]. The soil is considered as a cohesionless terrain, and the foundation is assumed as springs that are distributed entirely. The practicality of soft-soft and soft-stiff design methods is explored by Bisoi and Haldar [17, 18] when considering monopile-founded wind turbines established in clay, while they investigated the dynamic response of wind turbines rested on monopile foundation in clay under a combination of wave and wind loadings. To accommodate for soil nonlinearity, the pile strength to pile displacement was represented utilizing static *p-y*, *t-z*, and *q-z* curves in their model. In the frequency domain, Ghaemmaghami et al. [19] studied the seismic response of wind turbines that rested on a finite soft layer of soil. The soil beneath the foundation was defined by dynamic stiffness equations that were obtained following cone models.

Most conventional monopiles are used in the construction of foundations for wind turbines made from steel cylinder tubes. Some innovations were proposed to improve the lifespan of a wind turbine, such as using a double-skin steel tube with concrete poured between tubes in a transition piece or adding some internal restriction plates in the tubes to enhance the load-bearing capacity. Some researchers proposed a hybrid foundation with a monopile and a steel/concrete wheel located on the top segment of the monopile to reduce the rotation of the foundation. Li et al. [20] examined the utilization of restriction plates within the internal section of the monopile. In their study, they examined monopiles subjected to static loading and calculated their bearing capacity under the influence of gravity loading.

This paper investigates numerically the performance of an offshore wind turbine with a monopile foundation under the wind, wave, and seismic loadings. The monopile is equipped with an internal restriction plate (with four holes) at its middle height. The overarching goal of this study is to assess the dynamic responses of offshore wind turbines resting on such equipped monopiles in clayey soil under a combination loading of wind, wave, and earthquake. A fully solid model is used for modeling the monopile with an internal plate in ABAQUS/Explicit [21] software. This study contributes to the development of more efficient and resilient foundation design for offshore wind turbines.

2. Prototype Model

To research the feasibility of the monopile, a numerical study has been performed on the reference wind turbine with an output power of 5 MW (NREL (National Renewable Energy Laboratory)) [22, 23]. The main geometric characteristics of the reference turbine and the feature of the soft soil are summarized in Tables 1–3. To predict the monopile performance, 90 mm and 7500 mm were considered for the thickness and diameter of the wall, respectively.

3. Numerical Modeling

In this study, due to the complexity of the internal form of the monopile, using analytical models and beam elements in modeling cannot lead to a proper understanding of the differences in responses of wind turbines caused by changes in the structure of the monopile. Therefore, applying a solid 3D FE model with full details of the monopile can lead to a good insight into the behavior of the monopile-structure with different internal forms of monopile (Figure 1). In the FEM, the dimension of the soil part is 200 m × 200 m. At the bottom surfaces of the soil, a fixed constraint was considered, while boundary conditions for peripheral surfaces with infinite elements of the soil were selected as sliding supports. For modeling the soil, two types of elements including the C3D8R and the CIN3D8 are used. The element of CIN3D8 was used for the outer layer of the soil as an infinite element. The C3D8R element models the tube of the tower and other parts of the soil.

Table 1: Pile characteristics.

Parameters	Sign	Values
Total length of tower	L	113600 (mm)
Embedded depth (monopile)	L'	36000 (mm)
Exterior diameter	D	7500 (mm)
Thickness of pile wall	t_p	90 (mm)
Identical diameter	D_e	4100 (mm)
Young's modulus	E	2.1×10^8 (kPa)
Moment of inertia	I	14.84 (m^4)
Flexural rigidity	EI	3.12×10^9 ($kN{\cdot}m^2$)

Table 2: Key characteristics of the NREL 5 MW wind turbine with 3 blades.

Character	Amount
Diameter of the rotor (m)	126
Wind speed (m/s)	11.4
Cut-in, rated rotor speed (rpm)	6.9, 12.1
Rotor-nacelle mass (kg)	350,000
Diameter of tower base (mm)	6000
Thickness of tower base (mm)	27
Diameter of tower top (mm)	3870
Thickness of tower top (mm)	19
Coordinate location of RNA (x, y, z) (mm)	(410, 0.00, 1970)
Mass moment of inertia of RNA (x, y, z) ($kg{\cdot}m^2$)	(4.37, 3.35, $2.54) \times 10^7$
Mass of blade (kg)	17,740

3.1. Model Behavior of Materials

3.1.1. Soil. There have been many advances in modeling soil stress-strain behavior over the past 50 years. To demonstrate the behavior of soil in FE and finite difference methods regarding the soil-structure interaction issue, these developments and models are utilized. In several types of research, it was shown that applying the Mohr–Coulomb theory creates sensible results, but the analyses were conducted under monotonic loading and a small-strain range; as a result, this model cannot be used in seismic loading conditions. Based on research which was performed by Alisawi et al. [24], the differences between the reference and numerical models in which the Drucker–Prager model was used for soil material were smaller than those for the soil model with Mohr–Coulomb constitutive model. These models had less accuracy and represented that they were unsuitable for seismic loading conditions. Hence, the Cam-Clay model gives a reasonable response concerning a nonlinear elastic-hardening plastic behavior. Also, a gap-strike mechanism is implemented in the numerical model. The development of the gap occurs at an unlimited distance along the entire depth of the monopile. Therefore, piles have a wide area to deform laterally, and oscillation may happen. Once a gap is created between the soil and the monopile, the shear strength of the monopile peripheral surface is reduced as well as the capacity of the monopile and more distance is created between the two portions. This mainly applies to monopiles with a heavy weight load on the top layer of the system. In Table 4, the values of the parameters for the hardening law are presented.

3.1.2. Steel. There are several inelastic stress-strain constitutive model behaviors for steel materials. The most common usage of steel behavior is based on the general expression originally suggested by Ramberg and Osgood [25]. In (1), there are several variables in which E is Young's modulus, $\sigma_{0.2}$ is the yield stress, and n is the strain hardening exponent. The Ramberg–Osgood function is expressed as

$$\varepsilon = \frac{\sigma}{E} + 0.002\left(\frac{\sigma}{\sigma_{0.2}}\right)^n. \quad (1)$$

The J_2 flow theory [26, 27] was implemented to select the plastic behavior of the steel. The modulus of elasticity, Poisson's ratio, and yield stress for steel material which is used for tower, monopile, and internal plate are 210 GPa, 0.38, and 355 MPa, respectively.

3.2. Soil-Monopile Interaction, Solution Strategy, and Boundary Conditions.

The interaction between soil and pile or concrete and the pile is simulated by a formulation of a surface-to-surface in ABAQUS/Explicit [21]. In this method, the master surface is assigned to the surface of the monopile, and the surfaces of the foundation and soil which are in contact with the monopile are defined as the slave part [28]. A contact method, namely, a hard contact in the normal direction, is chosen for interaction among surfaces. Based on the literature [28–30], a Coulomb friction model can be used in the tangential direction to model the relationship between shear stress and gap. The friction coefficient between the monopile surface and soil is considered as $\tan(0.67 \times$ friction angle of soil). A reasonable value of 0.4 for the friction coefficient is selected [31].

There are four stages in the analysis. The first stage is the geostatic phase in which the body force of the soil is considered. In the second phase, to make stability between the monopile and the soil, the installation stage of the monopile is chosen. The static-friction loading step in the third phase by applying the gravity loads is accomplished. In the final phase, the dynamic analysis stage by applying wave and wind loading on the body of the tower and seismic loading to the lower part of the clay soil is performed. In dynamic analysis, to prevent the back reflection of the radiated waves, an infinite element was used in far distance areas.

In the geostatic and static steps, the deformations in the lateral direction were limited, while in the vertical direction, the displacement was free to move. At the lower part of the model, the support was selected as a fixed-roller constraint to simulate the shaking excitations.

3.3. Mesh Size.

The meshing process is one of the most important phases in numerical modeling. To a feasible model, the real state of the 3D soil-monopile model with brick types of elements, different types of the elements which are mentioned earlier, is used to mesh the parts of the system. A mesh with an element size of $0.55 \times 0.55 \times 0.35$ m was obtained for the area near the monopile to face the movement of the impedance deformation in a persistent way to the adjacent outer zone. A coarser mesh with the size of

Table 3: Soil characteristics [23].

Effective unit weight ($kN \cdot m^{-3}$)	Modulus of elasticity (MPa)	Angle of friction (deg.)	Cohesion (kPa)	Friction coefficient
10	30	33	2	0.4

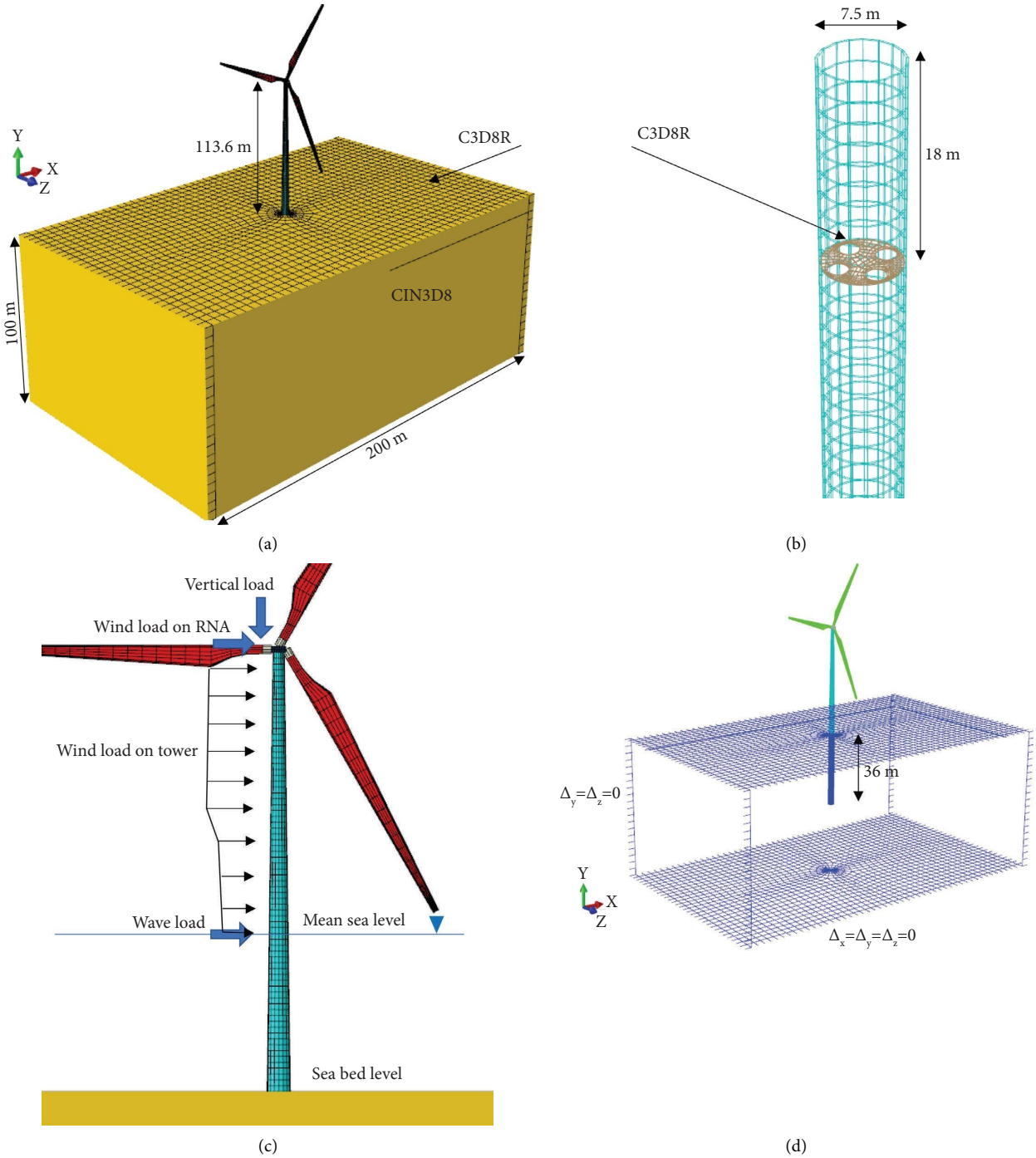

Figure 1: Schematic view of the wind turbine, assigning the elements and boundary conditions. (a) Meshed model with assigning the elements. (b) Wired mesh model of monopile with internal four-hole plate. (c) Loading on offshore wind turbine. (d) Boundary conditions and embedment length of monopile.

Table 4: Values of the parameters for the hardening law.

Logarithmic plastic bulk modulus	Stress ratio at critical state	Initial yield surface size (kPa)	Ratio of the flow stress in triaxial tension to the flow stress in triaxial compression
0.174	1	100	1

$2 \times 2 \times 1$ m was utilized in the far region. The strategy for choosing the mesh size is adopted by equation (2) in directions x and z. Equation (3) is considered for the corresponding far areas in horizontal directions and y-axis along the depth.

$$\Delta x = \left(\frac{1}{5} - \frac{1}{8}\right)\frac{C_m}{f_{\max}}, \tag{2}$$

$$\begin{aligned} \Delta x &= \left(\frac{1}{7}\right)l_w, \\ \Delta y &= \left(\frac{1}{8}\right)h_w, \end{aligned} \tag{3}$$

where C_m is the shear wave velocity, $f_{\max}$ is the maximum frequency, l_w is the average wavelength, and h_w is the average water depth of the site. Since using a very small mesh is impractical for many engineering problems and using a coarser mesh sometimes leads to an incorrect result, researchers usually try to adopt an appropriate mesh size. Therefore, the total number of nodes and the total number of elements are 96,608 and 89,553, respectively.

3.4. Loading Pattern

3.4.1. Permanent Load. The whole vertical load which is applied on the foundation depends on the total mass of the structural elements of the offshore wind turbine, a combination of the mass of the rotor-nacelle assembly (RNA), the mass of the tower's shaft, and the mass of the monopile.

3.4.2. Wind Load. Based on research which was performed by Arany et al. [32], the wind load applied on the turbine rotors is calculated using the following equation:

$$F_{\text{vh}} = 0.5\pi\rho_a R_T^2 V_{\text{hub}}^2 C_T, \tag{4}$$

where F_{vh} is the wind load applied on the rotor in N, ρ_a is the air density with the value of 1.25 kg/m^3, R_T is the internal radius of the rotor in m, V_{hub} is the wind speed at the top level of the tower in m/s, and C_T is the thrust factor, which is considered 1.0 for $V_{\text{hub}} = 11.4$ m/s in this study.

According to the ABS [33] regulations, to apply the wind load on the turbine tower body (F^z_{tower}), the tower can be divided into several segments, and the load can be exerted in each part.

$$F^z_{\text{tower}} = 0.5\rho_a A^z_{\text{tower}} V_z^2 C_s, \tag{5}$$

where A^z_{tower} is the surface of the tower under pressure in height z in m^2, C_s is shape factor which is 0.5 for cylindrical steel tubes, and z is the height from the seawater level to a particular level. The wind pattern (V_z) is a function of the height z. Based on the clauses on ABS [33], the standard wind profile is calculated as follows:

$$V_z = V_{\text{hub}}\left(\frac{z}{z_{\text{hub}}}\right)^{\beta}, \tag{6}$$

where z_{hub} is the height of the hub and the power-law exponent β depends on an irregular surface which is 0.12 in the open sea with waves [34].

3.4.3. Wave Load

$$F_{\text{hydro}} = F_{\text{Morison}} = F_D + F_I = 0.5\rho_w C_D A\left(v - u'\right)\left|v - u'\right| + \rho_w B\left(C_M v' - \left(C_M - 1\right)u''\right). \tag{7}$$

To calculate the wave load and hydrodynamic forces resulting from the interaction between water and the bottom part of the tower, the Morison equation has been used. The calculation of applied load from the wave on cylindrical components depends on the ratio of wavelength to the diameter of the member [35]. Wave load can be calculated by summing the drag and inertia forces.

F_{hydro} is the hydrodynamic load, F_D is the drag force acting on the member axis, F_I is an inertia force matrix, ρ_w is the density of water, A is a reflected surface on the cylindrical axis, B is the transferred volume of the cylinder in the length unit, C_D is the drag coefficient, C_M is an inertia coefficient, v is a velocity vector component perpendicular to the member axis, v' is an acceleration vector component in m/s^2, u' is the velocity of structure response in m/s, and u'' is the acceleration of structure response.

3.4.4. Seismic Load. The earthquake records correspond to the Northridge event of 1994 in the San Fernando Valley region of the city of Los Angeles and are used to conduct free field analysis. The magnitude of the record was 6.7, and the maximum horizontal acceleration was 0.843 g. The acceleration time history of the record of Northridge is depicted

in Figure 2. Furthermore, the 22 far-field records which are presented in the FEMA-P695 [36] are also selected to study the dynamic behavior of the wind turbine under a combination of wind, wave, and seismic loading. Figure 3 depicts the distribution of the internal responses along the soil depth with a maximum acceleration of 0.5 g for the seismic record.

3.5. Damping. Several parameters of damping, including aerodynamic, hydrodynamic, material, and radiation damping, influence the total value of damping of the structure. Based on the guidelines [34], the steel damping from internal friction is in the range of 0.2% and 0.3%. Veletsos [37] and Gazetas [38] depicted that the soil had a maximum portion of damping in the wind turbine system, and in some cases, it can pass from 20% regarding the medium base. According to research which was performed by Lombardi et al. [39], the material damping rises corresponding to the load cycles. Hence, the value of 8% for soil and steel materials is selected. For an aerodynamic damping value, a value of 3.5% with a low wind speed is considered. Based on the GL regulations, the values of 0.15% and 0.22% are selected for hydrodynamic and radiation damping. As a result, a total damping of 12% damping is applied.

4. Validation of the Numerical Model

To investigate the behavior of a monopile foundation equipped with a restriction plate inside the monopile, an experimental study [20] was chosen. The diameter, overall length, and embedment depth of the steel monopile were 1.27 m, 8.65 m, and 4.00 m, respectively. A static load type was applied as a monotonic pattern. Figure 4 represents a comparison between the results of the numerical model and the test sample. The maximum difference between the experimental and numerical results in terms of initial stiffness for pipe pile and four-hole type was 3.7% and 4.8%, respectively.

5. Results and Discussion

In Section 5.1, the behavior of turbine structures under wind load is studied. Then, in Section 5.2, the behavior of the turbine tower under wave load is investigated. The behavior of turbines under earthquake load is investigated in Section 5.3. In these sections, the soil characteristics are constant as illustrated in Table 3. Assuming that all parameters are constant, the soil properties in Section 5.4 were changed to investigate their effect on wind turbine behavior. In Section 5.5, with a combination of wind and wave loadings, the responses of the turbine and soil are investigated. A full combination of loading, including wind, wave, and earthquake, is applied to the model in Section 5.6 to investigate the behavior of the offshore wind turbine.

5.1. Response of Turbine under Wind Load Only. In this section, four values of wind velocities (V_s) are considered, including 3 m/s, 6 m/s, 12 m/s, and 20 m/s. The distribution of displacement, bending moment, and acceleration along the tower and monopile height is represented in Figure 5. In Figure 6, the distribution of displacement at 5 segments of the tower body based on different wind velocities is shown. According to Figure 6, the maximum displacement occurred at the hub with 0.79 m when the wind velocity was 20 m/s. This is around 10 times the displacement of the hub when the wind velocity was 3 m/s. The maximum deformation of the turbine tower was in the top third segment. Also, with increasing wind velocity, the lower part of the monopile tends to move, and it shifted from 2.5 mm to 30.8 mm at the base ($h = 0$) when the wind velocity increased from 3 m/s to 20 m/s. Figure 7 shows the distribution of displacement, bending moment, and acceleration along the turbine height under the wind load with a velocity of 20 m/s, which is distributed on the tower (F_{tower}), and the wind load is applied on the hub (F_{vh}), and the combination of both these loadings. Based on the result, the wind velocity had a substantial effect on the offshore wind turbine behavior. As can be seen from Figure 7, the wind load acting on the turbine tower had a minor effect on the turbine response, while the major portion of the structural response of the turbine was related to the wind acting on the hub and rotor.

Equation (8) indicates the changes in C_T concerning the induction factor (α). Different analyses were conducted to investigate the sensitivity of the results by changing the induction factor.

$$C_T = 4\alpha(1 - \alpha). \tag{8}$$

Figure 8 shows the maximum displacement at different levels of turbine height and different wind velocities. It can be seen that by increasing the thrust coefficient, the response of the turbine tower in terms of displacement had a reverse trend. After passing the value of the induction factor from 0.5, the thrust coefficient decreased; as a result, a value of 0.5 was selected for the previous analyses. In Figure 9, the wind load distribution along the tower height for four different values of wind velocity is shown. According to this figure, the vertical wind velocity that led to the vortex shedding phenomenon is in the range of 3 m/s to 10 m/s. Furthermore, with increasing wind velocity, the region of the wind resonance will move from the top segment of the tower to the lower part of the tower.

5.2. Response of Turbine under Wave Load Only. There are two key parameters for considering the wave load, including wave height (H_s) and wave period (T_s). Among these parameters, the effect of wave height on tower behavior is too clear, and the displacement of the tower will increase by increasing the wave height. Hence, the parameter of wave period is selected only for parametric study in this section. Three values of 5 sec, 8 sec, and 11 sec of wave period with a fixed value of wave height (5 m) are considered. The maximum displacement, distribution of bending moment, and acceleration profile are represented in Figure 10. Based on the result, the period of a wave has a substantial effect on the turbine tower behavior. This effect is due to the influence of wave period on the wave load of the cylindrical type of the tower. By increasing the wave period, the response of the tower will decrease.

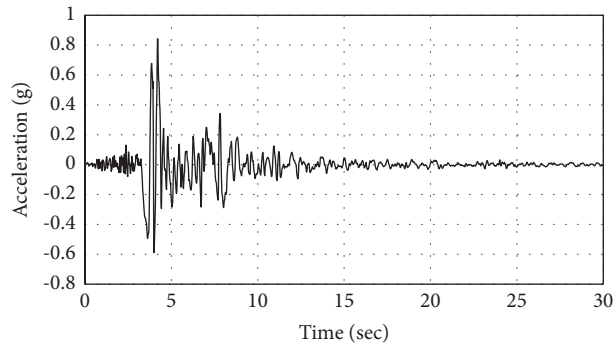

Figure 2: Time history acceleration of Northridge record.

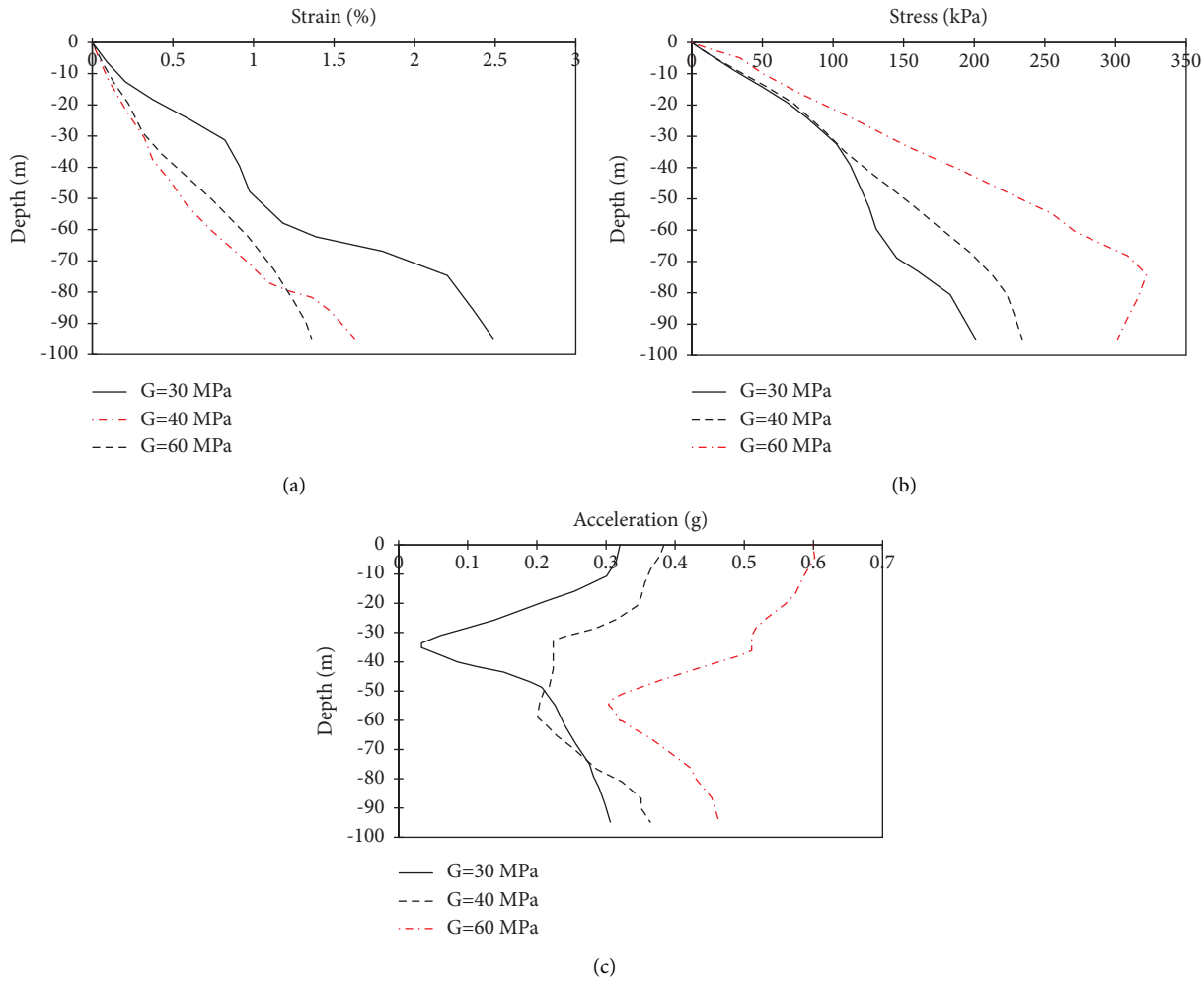

Figure 3: Distribution of strain, stress, and acceleration over the soil depth. (a) Distribution of strain. (b) Distribution of stress. (c) Distribution of acceleration.

5.3. Response of Turbine under Earthquake Load Only. Two parameters of the maximum acceleration of seismic record and shear modulus of the soil play an important role in the tower behavior. It is well known that with increasing the peak ground acceleration, the response of the turbine tower will grow. Hence, in this study, the parameter of the soil shear modulus with three different values of 20 MPa, 50 MPa, and 70 MPa and a constant value of 0.7 g for peak ground motion is considered for parametric study. The profiles of displacement, bending moment, and acceleration over the tower are drawn in Figure 11. Based on the result, it can be found that the shear modulus has a substantial role in the tower response. Increasingly, the highest values of displacement and bending moment decreased by increasing the

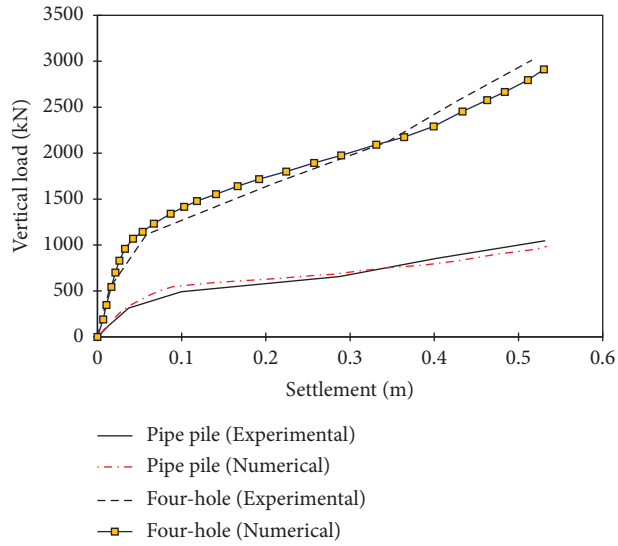

Figure 4: A comparison of the vertical load-settlement curve between experimental and numerical results.

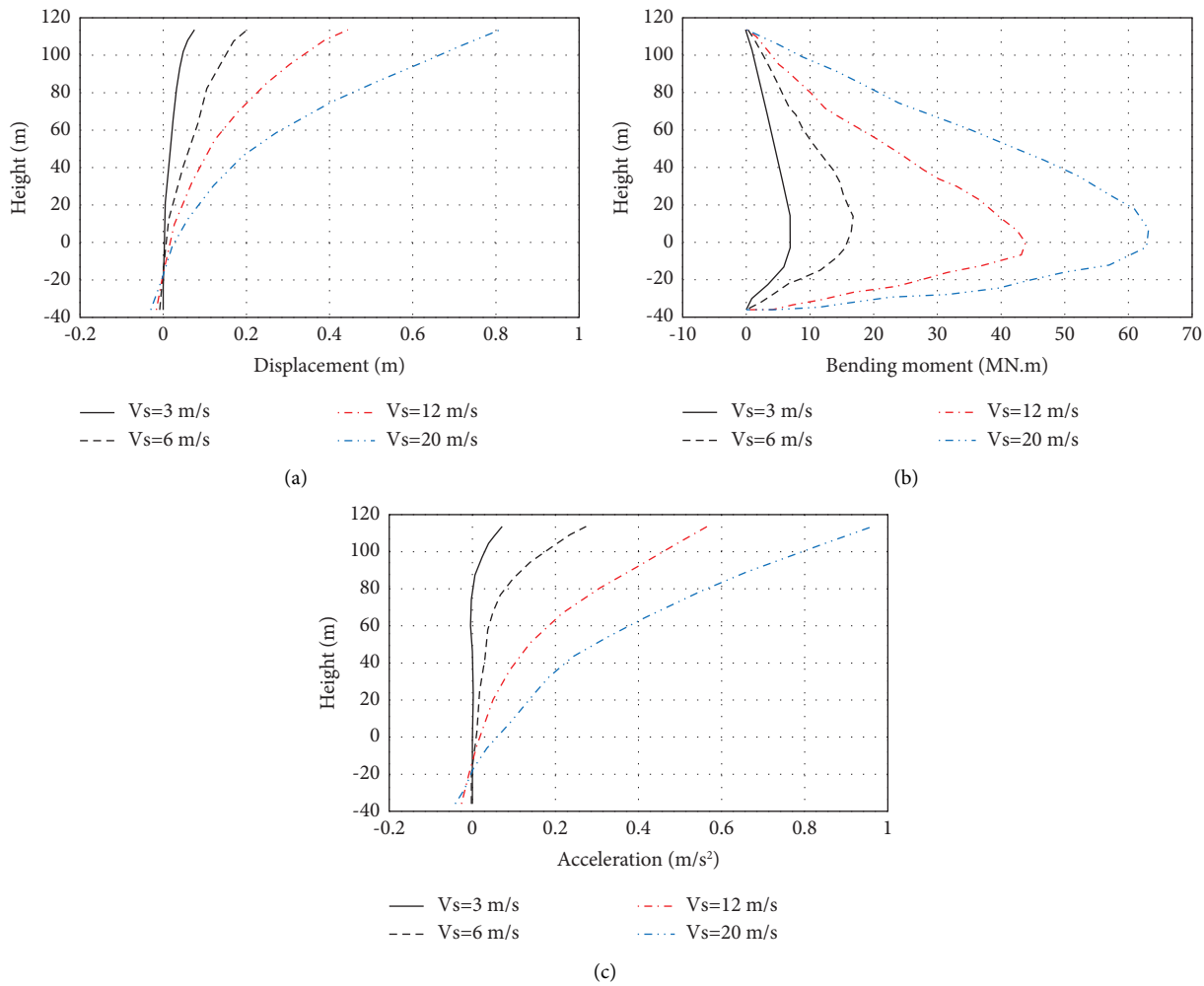

Figure 5: Distribution of (a) displacement, (b) bending moment, and (c) acceleration of the turbine under different values of wind velocity.

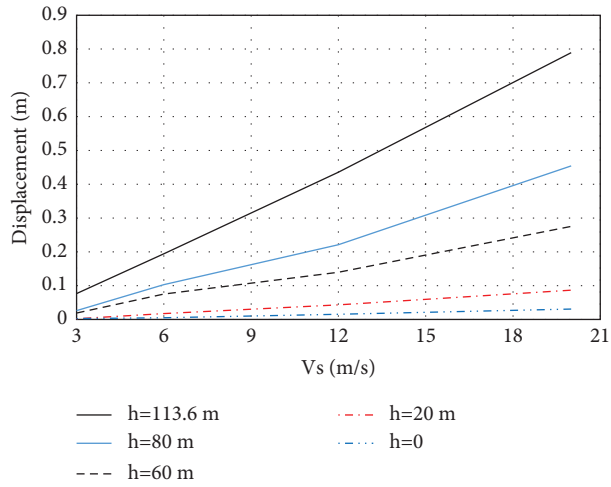

Figure 6: Maximum displacement variation of different levels of the tower.

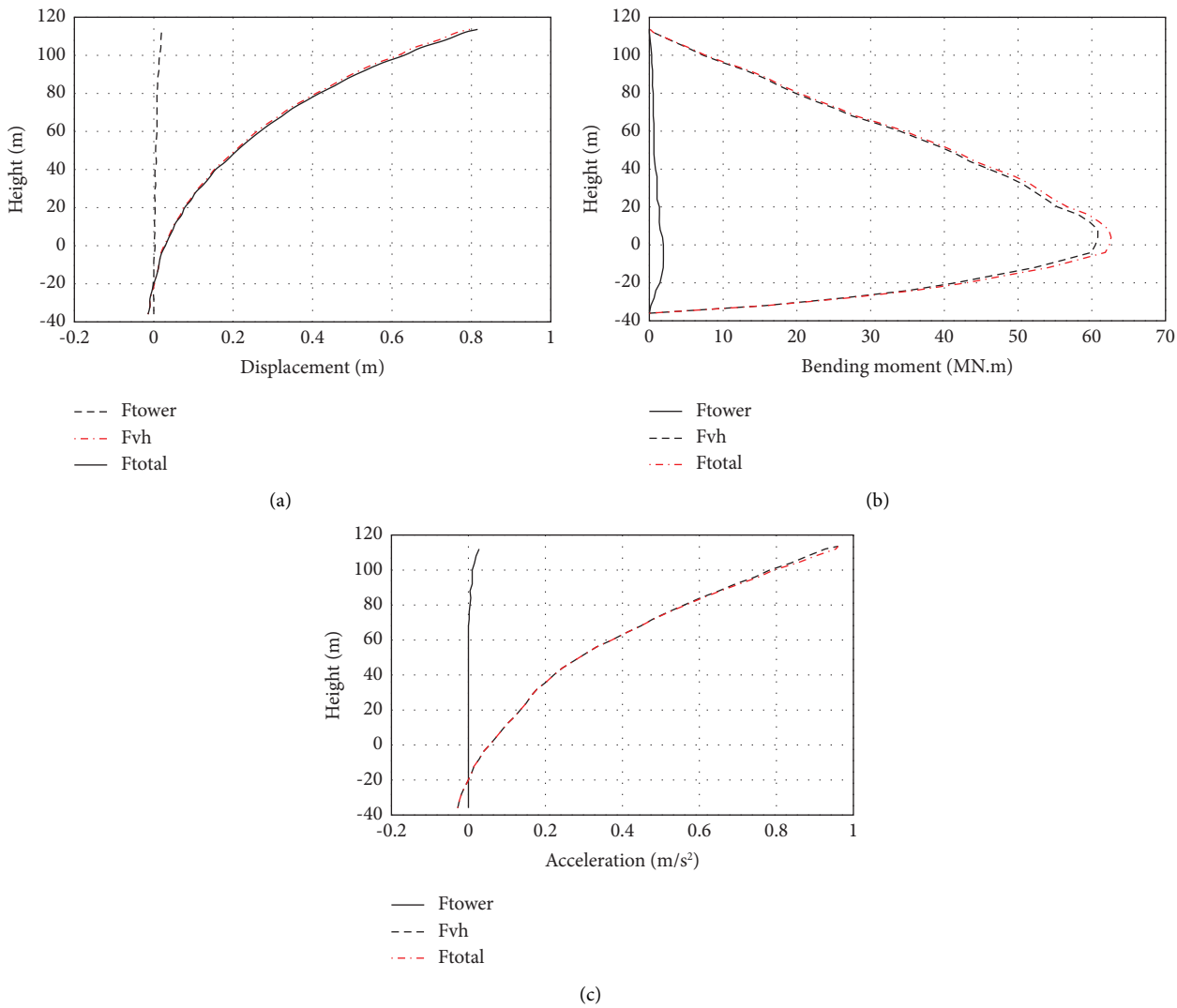

Figure 7: A comparison between the distributed wind force along the tower height and concentrated wind force on the hub in terms of (a) displacement, (b) bending moment, and (c) acceleration.

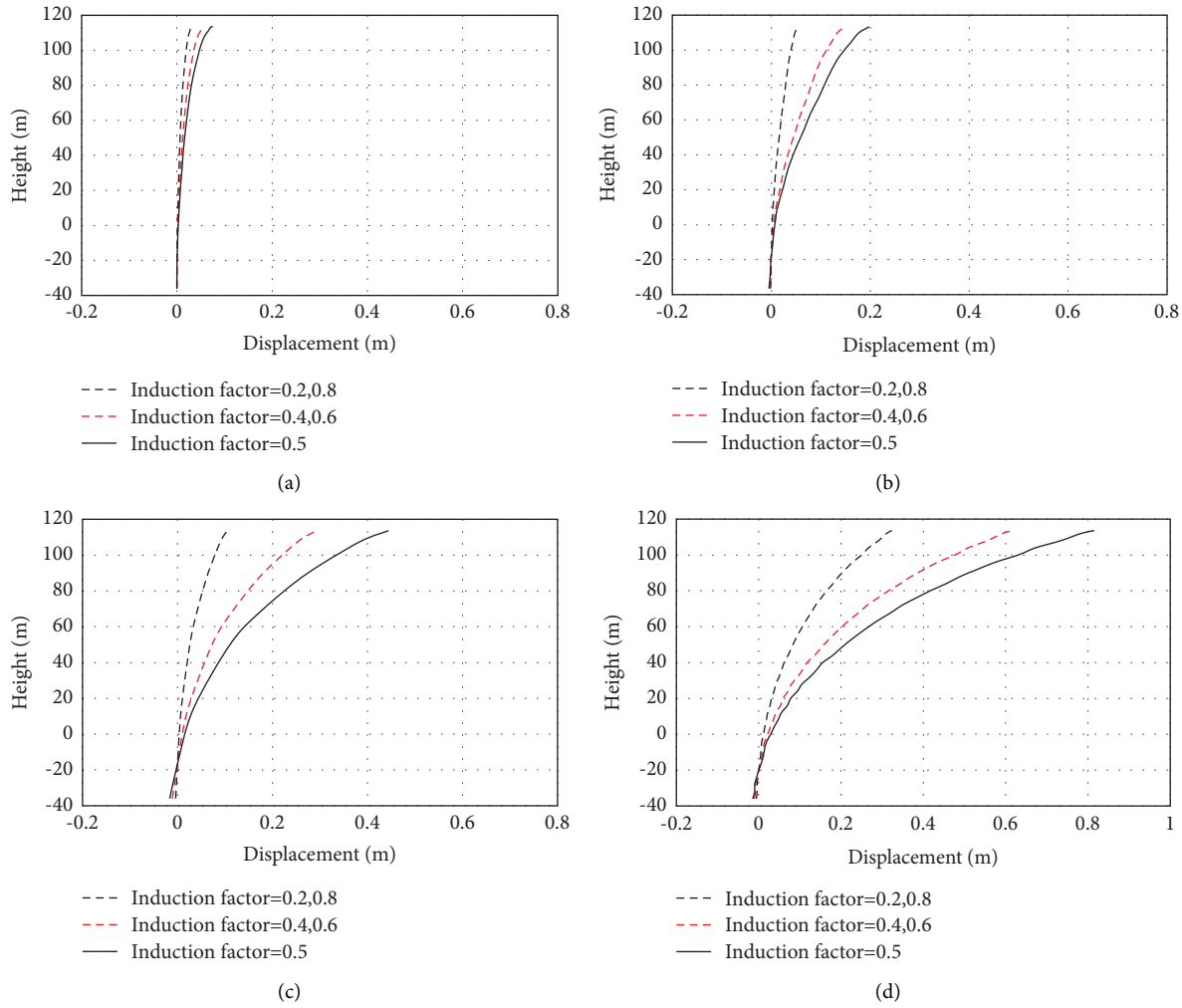

Figure 8: Displacement of the tower and monopile shaft under different wind velocities and various induction factors. (a) $V_s = 3$ m/s. (b) $V_s = 6$ m/s. (c) $V_s = 12$ m/s. (d) $V_s = 20$ m/s.

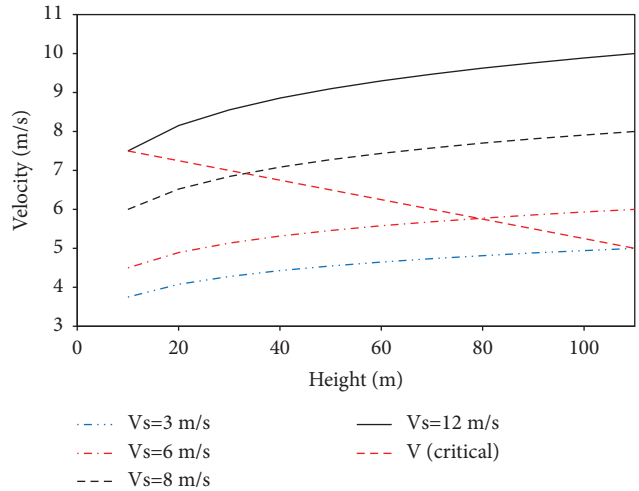

Figure 9: Profile of wind velocity and critical wind velocity throughout the tower body.

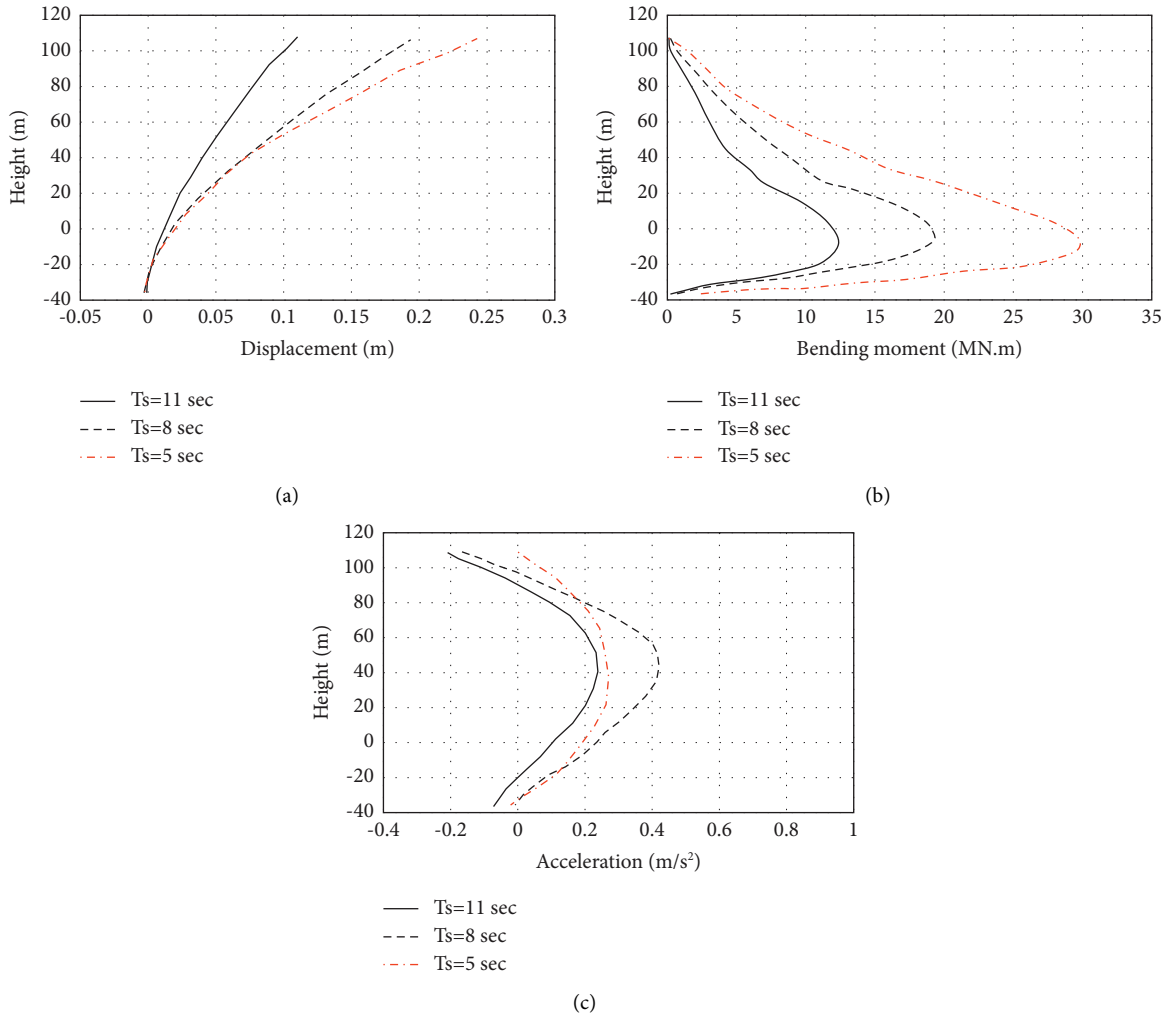

FIGURE 10: Distribution of (a) displacement, (b) bending moment, and (c) acceleration over the tower and monopile under various values of wave periods.

shear modulus, while the peak acceleration increased. This is due to the decreasing displacement of the soil in accordance with the increasing acceleration of the soil.

5.4. Effect of Soil Properties. In the region of the ocean with a depth lower than 30 m, the offshore wind turbine's foundation is embedded in clay soil. Four different values of undrained shear strength of clay soil (10 kPa, 30 kPa, 50 kPa, and 70 kPa) are considered to study the effect of the parameter on the turbine tower response. The maximum displacement at the turbine's hub and maximum bending moment at the bottom part of the tower are shown in Figure 12. With increasing undrained shear strength of clay, the maximum displacement at the top level of the tower has a declining trend in both wind and wave loading. This is mainly because both loadings are applied to the tower body, and by increasing the shear strength of clay, the base of the tower closes to the fixed base. Seismic loading is a form of input energy that is applied at the seabed, and it has the ability to amplify acceleration and cause changes in soil characteristics. Due to the effects of seismic loading, the displacement profile of offshore structures may exhibit different trends than those under other types of loading. Increasing the shear strength of clay can result in an increase in the natural frequency of the system. This increase in frequency is particularly noticeable at the third frequency, as the stiffness of the soil is highest at that frequency.

In all previous investigations, the strain in half of the peak stress on the undrained compression test of soil (ε_{50}) was 0.005, and Matlock suggested that ε_{50} has a range of 0.005–0.02. Hence, five values of 0.005, 0.008, 0.01, 0.015, and 0.02 are selected for studying the effect of ε_{50} on the behavior of the system. It can be seen from Figure 13 that ε_{50} has a key role in the behavior of the system. By increasing ε_{50}, the maximum displacement at the top level of the turbine tower increases under wind and wave loadings while the trend of displacement at the top part of the tower has a reverse pattern, and it reaches from around 0.6 m to 0.5 m at a value of 0.02 for ε_{50}. Interestingly, the maximum bending moment at the seabed decreased from 105 MN·m to around 90 MN·m (decreased by 15%) under seismic loading,

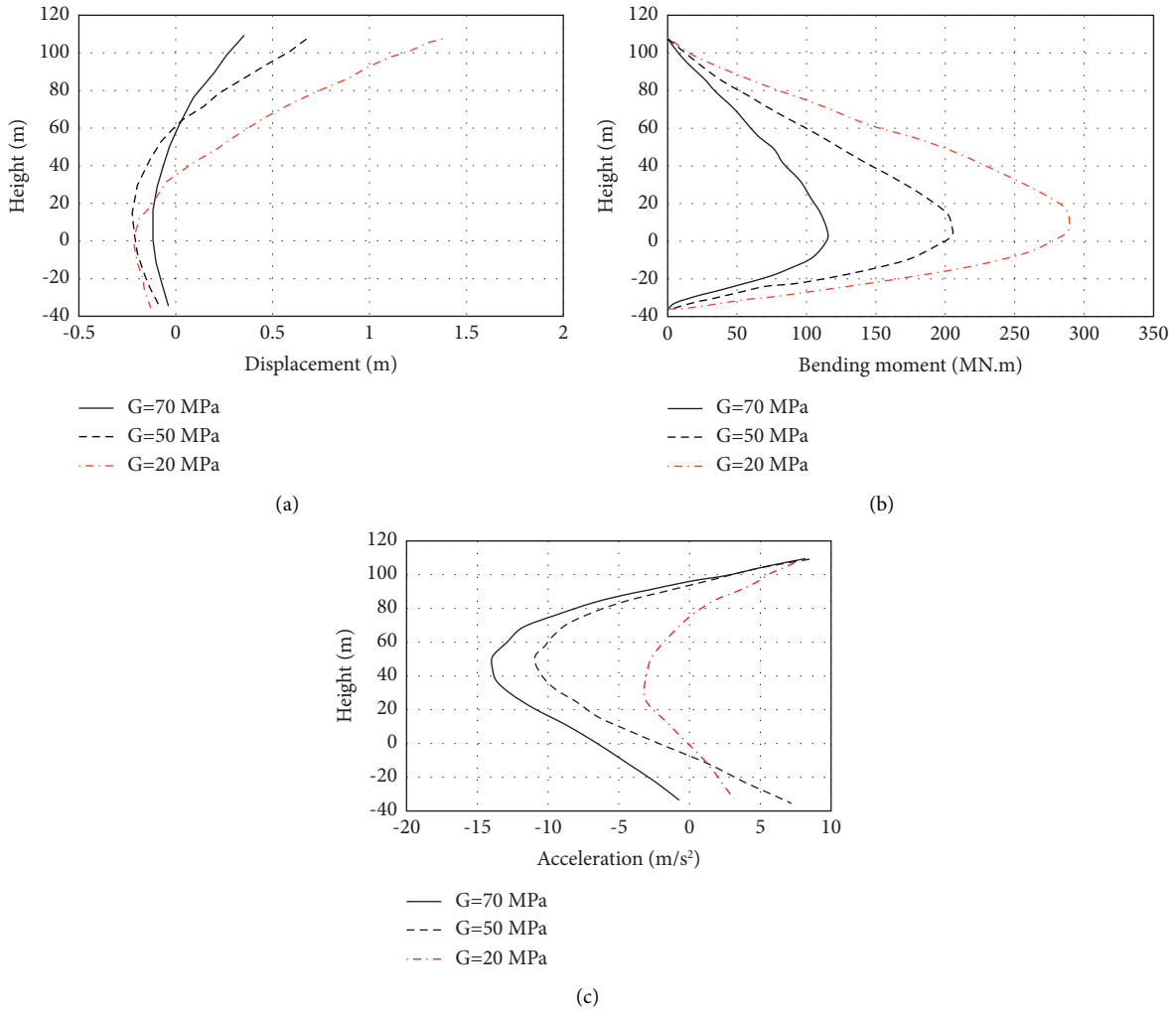

Figure 11: Distribution of (a) displacement, (b) bending moment, and (c) acceleration over the tower and monopile under various values of the undrained shear modulus of soil.

while the other two types of loadings had no substantial effect on the system response. Furthermore, there is an inverse trend between the frequency and ε_{50} values. It can be seen that the value of frequency decreased from 3.70 Hz to 3.06 Hz in the third mode.

5.5. Response of Turbine under a Combination of Wind and Wave Loadings. Figure 14 shows the effect of wave loading on the system behavior under a combination of wind and wave loadings. In the vertical axis, three dimensionless parameters are defined as λ_d, λ_a, and λ_b. These parameters are the ratio of the peak displacement, maximum acceleration at the top part of the tower, and the peak bending moment at the seabed level under wind loading to that under a combination of loadings. From Figure 14, it can be seen that the weak wind with a speed of 3 m/s and wave height of 6 m has a substantial effect on the system behavior, whereas the strong wind with different induction factors has little effect on the tower's behavior. For instance, when the wave height is 1 m, λ_d is around 1.75 corresponding to a wind velocity of 20 m/s and it reaches approximately 6.5 corresponding to a wave height of 6 m. Figure 15 depicts the response of the system for different periods at a wind velocity of 12 m/s. The fundamental period of the system is represented by T_f in the figure, and T_s represents the significant wave period. At a value of 1.50 for T_s/T_f, the maximum value for each of the ratios can be achieved. The main reason for this is that the wave load elevates initially, and the drops correspond to increasing wave period, and it obtains its highest values when the period of the wave is around 5.5 sec. Based on the results, the combined effect of wave and wind loadings should be implemented for practical applications and designing the turbine system.

5.6. Response of Turbine under a Combination of Wind, Wave, and Seismic Loadings. Figure 16 depicts the influence of earthquake loading on the system under a combination of three types of loadings. To study the intended issue, 22 far-field records with a magnitude range from M6.5 to M7.6 that happened between 1971 and 1999 are chosen from FEMA P695 [36]. It can be concluded that the displacement and bending moment at a small peak acceleration (0.1 g) are

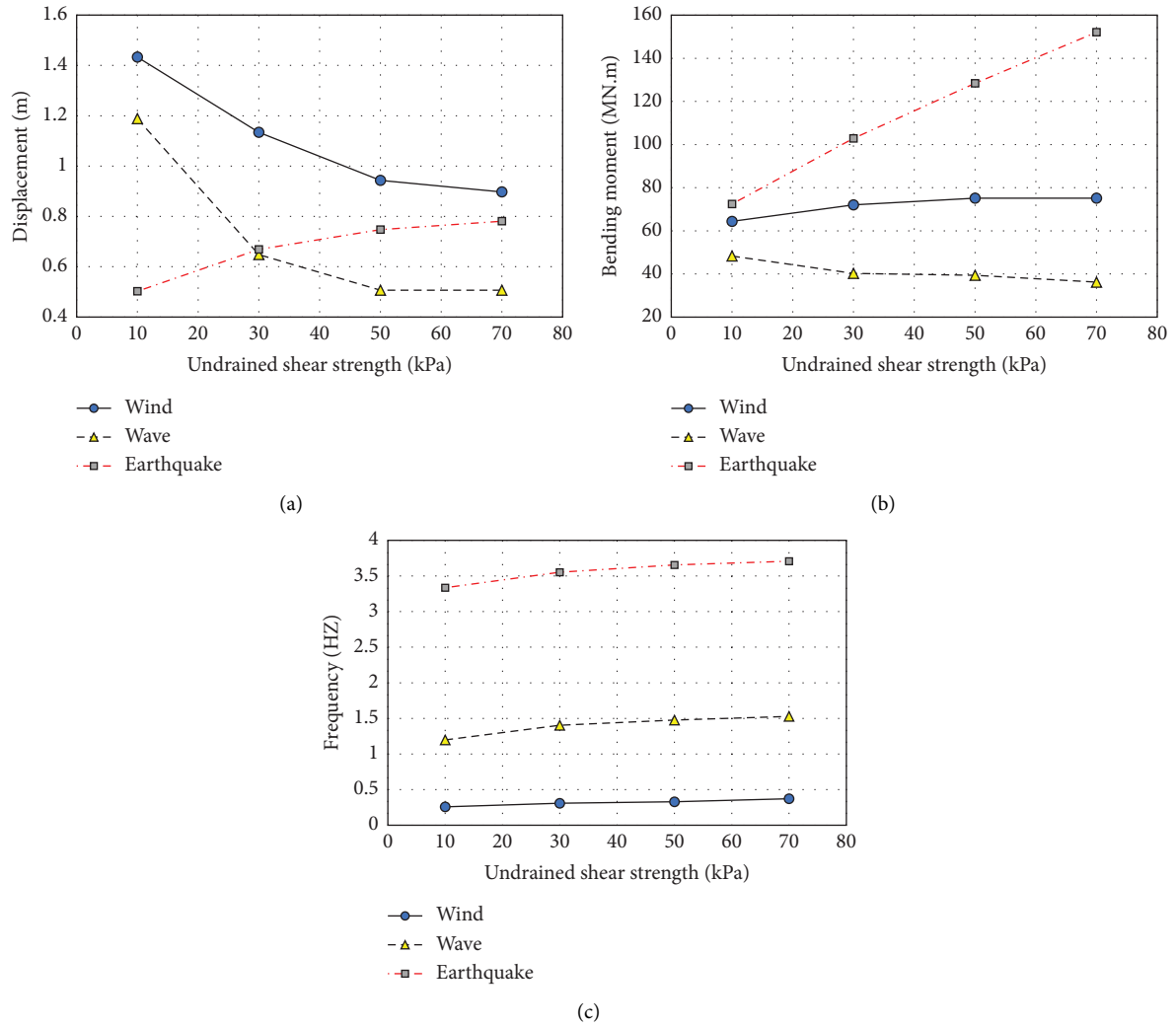

Figure 12: Distribution of (a) displacement, (b) bending moment, and (c) frequency versus undrained shear strength of the clayey soil under various loadings.

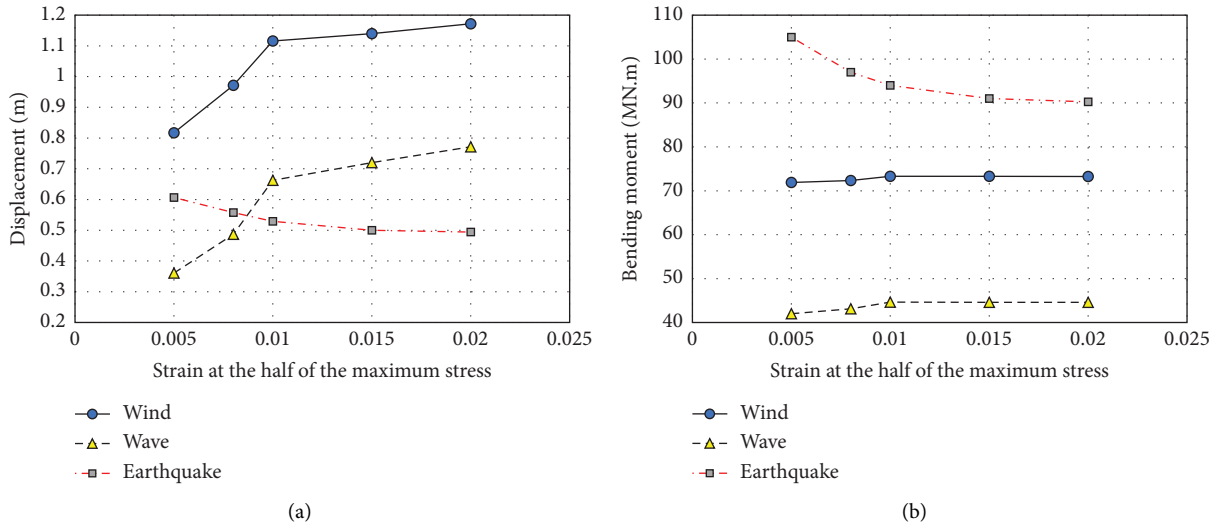

Figure 13: Continued.

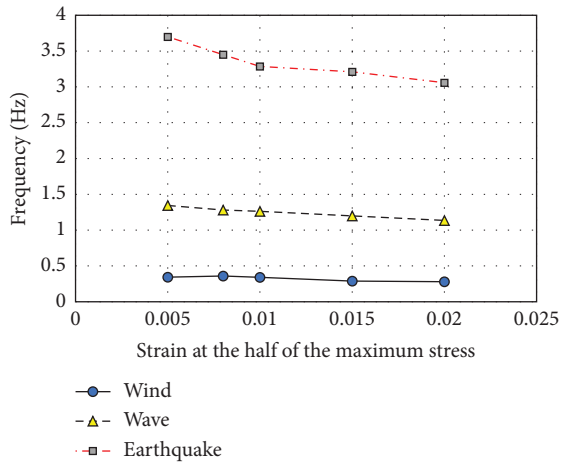

(c)

Figure 13: Distribution of (a) displacement, (b) bending moment, and (c) frequency versus strain at half of the maximum stress under the wind, wave, and seismic loadings.

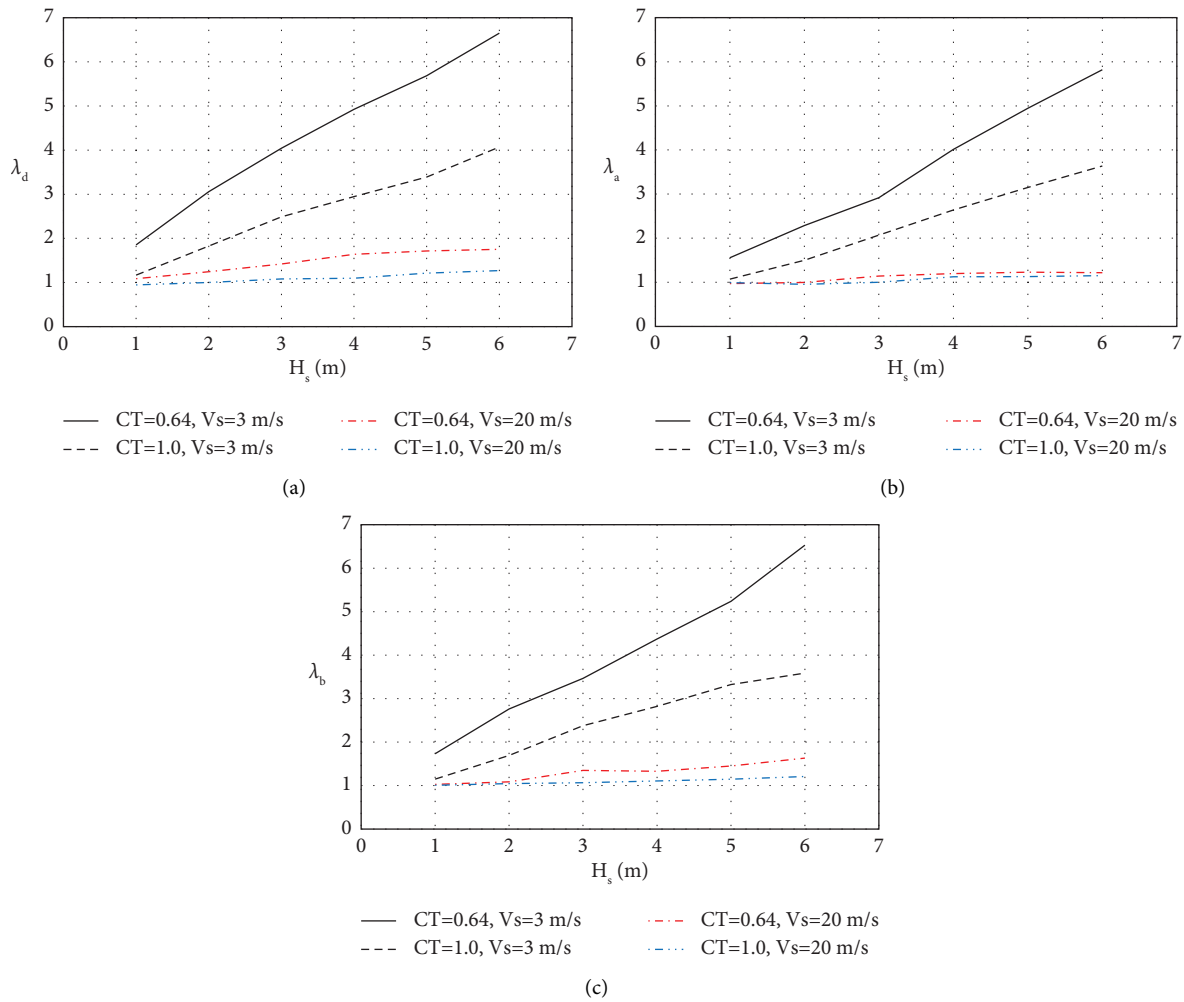

Figure 14: Variation of (a) λ_d, (b) λ_a, and (c) λ_b versus wave height under different wind velocities and induction factors.

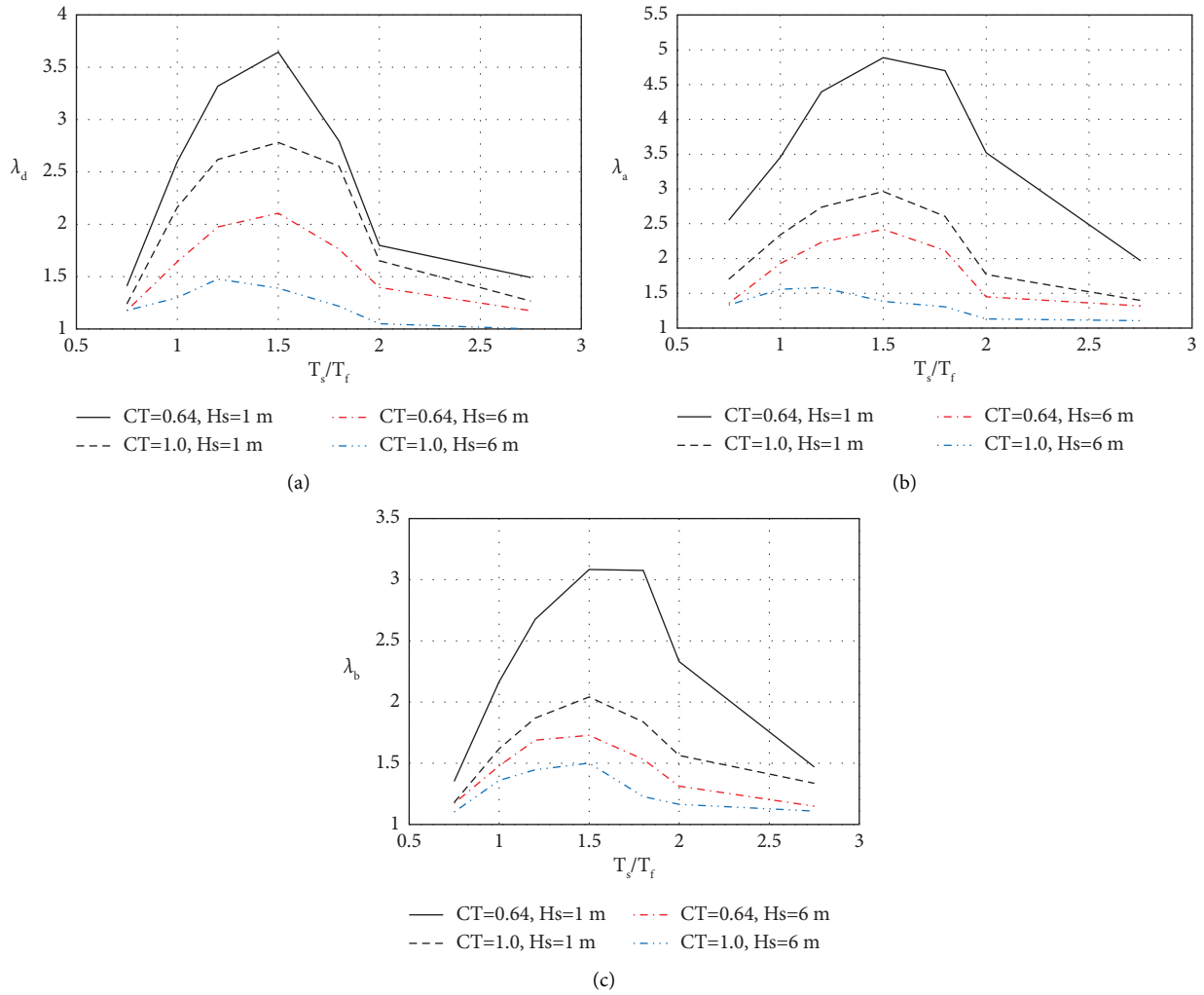

Figure 15: Variation of (a) λ_d, (b) λ_a, and (c) λ_b versus the ratio of the significant period to the fundamental period under different wave heights and induction factors.

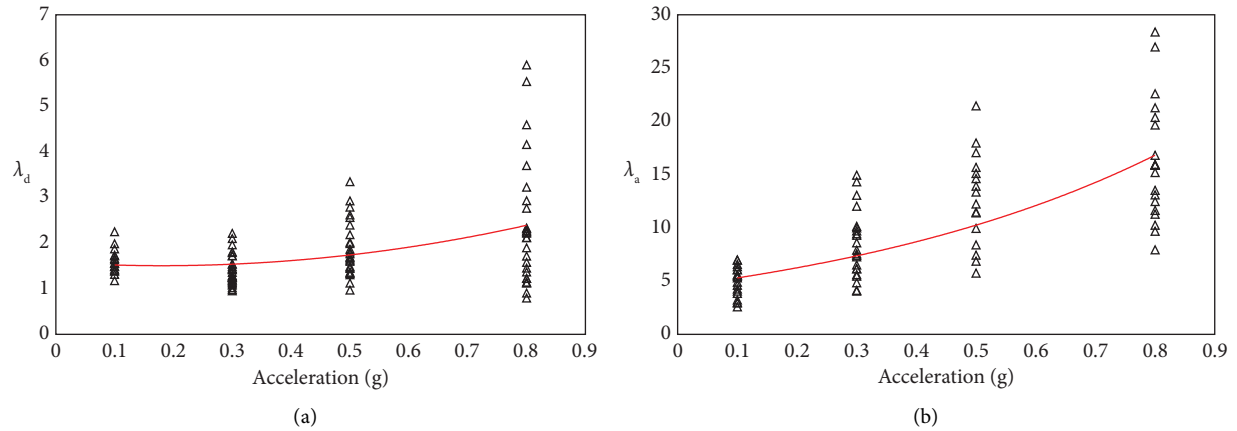

Figure 16: Continued.

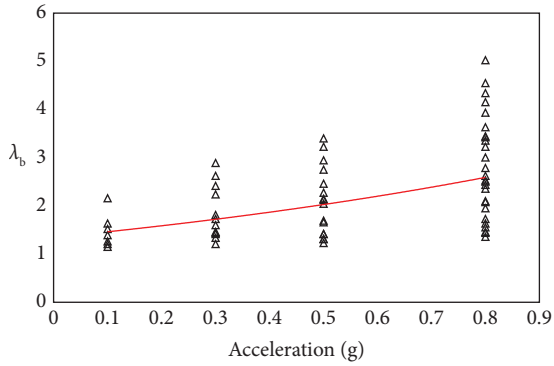

(c)

Figure 16: Effect of earthquake action on (a) λ_d, (b) λ_a, and (c) λ_b of the system subjected to combined wind, wave, and seismic loadings.

attributable to wave and wind loadings, whereas the responses under a combination of three loadings at a large seismic acceleration (0.8 g) are more caused by seismic loading. Consequently, it is necessary to consider the effect of all loadings on the response of the system.

6. Conclusions

A numerical model of an offshore wind turbine with a monopile foundation equipped with an inside restriction plate under a combination of loadings considering soil-monopile-tower-water interaction is represented. The effect of several parameters, including soil features, wind speed, the height of the wave, the period of the wave, and the effect of loading type on the behavior of the system, is considered in this study. A synopsis of the main findings can be presented as follows:

(a) By increasing wind velocity, the responses of the turbine tower increase. Also, the wind load acting on the hub had the most important effect on the response of the system rather than the distributed wind load acting on the tower. Using a value of 0.5 for the induction factor had the highest effect on the turbine responses, and the wind resonance shifted from the top part to the lower part of the tower when the wind velocity increased.

(b) When the turbine tower is exposed to the wave load only, the response of the turbine had a decreasing trend with the increase of the wave period. On the other hand, the maximum displacement and bending moment of the system under earthquake loading only decreased with the increase of the soil shear modulus while the peak acceleration increased.

(c) With a constant set of parameters, by increasing the shear modulus of the clayey soil, the maximum displacement at the hub part of the turbine decreased under wind and wave loadings while it increased under seismic loading. This is mainly due to the difference between the location of applied loadings and their inherent features. Furthermore, the overall trend of frequency was decreased with the increase of the strain corresponding to one-half the maximum stress.

(d) In terms of a combination of wind and wave loadings, the results revealed that the weak wind and the maximum height of the wave had a substantial effect on the turbine behavior rather than that of the strong wind with a minimum height of the wave. Also, the maximum value of responses occurred at a value of 1.50 for T_s/T_f. With adding a seismic load to other types of loadings, the movement and bending moment at a small peak acceleration (0.1 g) are attributable to wave and wind loadings, whereas the responses under a combination of three loadings at a large seismic acceleration (0.8 g) are more caused by seismic loading.

Data Availability

The data used to support the findings of this study are included within the article.

Conflicts of Interest

The authors declare that they have no conflicts of interest.

Authors' Contributions

Both authors have significantly contributed to the development and the writing of this research article. MEJ and DPNK were responsible for conceptualization, methodology, software, validation, formal analysis, investigation, resources, data curation, visualization, original draft preparation, and review and editing. DPNK was responsible for project administration and supervision. Both authors have read and approved the final manuscript.

References

[1] G. Cortina, V. Sharma, R. Torres, and M. Calaf, "Mean kinetic energy distribution in finite-size wind farms: a function of turbines' arrangement," *Renewable Energy*, vol. 148, pp. 585–599, 2020.

[2] X. Wang, X. Zeng, X. Li, and J. Li, "Investigation on offshore wind turbine with an innovative hybrid monopile foundation: an experimental based study," *Renewable Energy*, vol. 132, pp. 129–141, 2019.

[3] M. Bilgili, A. Yasar, and E. Simsek, "Offshore wind power development in Europe and its comparison with onshore counterpart," *Renewable and Sustainable Energy Reviews*, vol. 15, no. 2, pp. 905–915, 2011.

[4] X. Wang, X. Zeng, X. Yang, and J. Li, "Seismic response of offshore wind turbine with hybrid monopile foundation based on centrifuge modelling," *Applied Energy*, vol. 235, pp. 1335–1350, 2019.

[5] R. Mo, R. Cao, M. Liu, and M. Li, "Effect of ground motion directionality on seismic dynamic responses of monopile offshore wind turbines," *Renewable Energy*, vol. 175, pp. 179–199, 2021.

[6] F. Liang, Z. Yuan, X. Liang, and H. Zhang, "Seismic response of monopile-supported offshore wind turbines under combined wind, wave and hydrodynamic loads at scoured sites," *Computers and Geotechnics*, vol. 144, Article ID 104640, 2022.

[7] R. Xi, C. Xu, X. Du et al., "Framework for dynamic response analysis of monopile supported offshore wind turbine excited by combined wind-wave-earthquake loading," *Ocean Engineering*, vol. 247, Article ID 110743, 2022.

[8] D.-P. N. Kontoni and A. A. Farghaly, "Assessing seismic mitigation schemes of tuned mass dampers for monopile offshore wind turbine including pile–soil–structure interaction," *Asian Journal of Civil Engineering*, vol. 25, no. 2, pp. 1773–1799, 2023.

[9] X. Cheng, T. Wang, J. Zhang, P. Wang, W. Tu, and W. Li, "Dynamic response analysis of monopile offshore wind turbines to seismic and environmental loading considering the stiffness degradation of clay," *Computers and Geotechnics*, vol. 155, Article ID 105210, 2023.

[10] R. Kourkoulis, P. Lekkakis, F. Gelagoti, and A. Kaynia, "Suction caisson foundations for offshore wind turbines subjected to wave and earthquake loading: effect of soil–foundation interface," *Géotechnique*, vol. 64, no. 3, pp. 171–185, 2014.

[11] R. A. Kjørlaug and A. M. Kaynia, "Vertical earthquake response of megawatt-sized wind turbine with soil-structure interaction effects," *Earthquake Engineering and Structural Dynamics*, vol. 44, no. 13, pp. 2341–2358, 2015.

[12] S. Corciulo, O. Zanoli, and F. Pisanò, "Transient response of offshore wind turbines on monopiles in sand: role of cyclic hydro–mechanical soil behaviour," *Computers and Geotechnics*, vol. 83, pp. 221–238, 2017.

[13] F. Taddei, C. Butenweg, and S. Klinkel, "Parametric investigation of the soil–structure interaction effects on the dynamic behaviour of a shallow foundation supported wind turbine considering a layered soil," *Wind Energy*, vol. 18, no. 3, pp. 399–417, 2015.

[14] S. Adhikari and S. Bhattacharya, "Dynamic analysis of wind turbine towers on flexible foundations," *Shock and Vibration*, vol. 19, no. 1, pp. 37–56, 2012.

[15] M. Feyzollahzadeh, M. Mahmoodi, S. Yadavar-Nikravesh, and J. Jamali, "Wind load response of offshore wind turbine towers with fixed monopile platform," *Journal of Wind Engineering and Industrial Aerodynamics*, vol. 158, pp. 122–138, 2016.

[16] S. Darvishi-Alamouti, M.-R. Bahaari, and M. Moradi, "Natural frequency of offshore wind turbines on rigid and flexible monopiles in cohesionless soils with linear stiffness distribution," *Applied Ocean Research*, vol. 68, pp. 91–102, 2017.

[17] S. Bisoi and S. Haldar, "Dynamic analysis of offshore wind turbine in clay considering soil–monopile–tower interaction," *Soil Dynamics and Earthquake Engineering*, vol. 63, pp. 19–35, 2014.

[18] S. Bisoi and S. Haldar, "Design of monopile supported offshore wind turbine in clay considering dynamic soil–structure-interaction," *Soil Dynamics and Earthquake Engineering*, vol. 73, pp. 103–117, 2015.

[19] A. R. Ghaemmaghami, O. Mercan, and R. Kianoush, "Seismic soil–structure interaction analysis of wind turbines in frequency domain," *Wind Energy*, vol. 20, no. 1, pp. 125–142, 2017.

[20] J. Li, X. Wang, Y. Guo, and X. B. Yu, "The loading behavior of innovative monopile foundations for offshore wind turbine based on centrifuge experiments," *Renewable Energy*, vol. 152, pp. 1109–1120, 2020.

[21] Abaqus, *ABAQUS Analysis User's Manual, Version 6.14*, Dassault Systemes Simulia Corp, Providence, RI, USA, 2014.

[22] J. M. Jonkman, *Dynamics Modeling and Loads Analysis of an Offshore Floating Wind Turbine*, National Renewable Energy Laboratory, Golden, CO, USA, 2007.

[23] H. Ma and J. Yang, "A novel hybrid monopile foundation for offshore wind turbines," *Ocean Engineering*, vol. 198, Article ID 106963, 2020.

[24] A. Alisawi, P. Collins, and K. Cashell, "Nonlinear numerical simulation of physical shaking table test, using three different soil constitutive models," *Soil Dynamics and Earthquake Engineering*, vol. 143, Article ID 106617, 2021.

[25] W. Ramberg and W. R. Osgood, "Description of stress-strain curves by three parameters," Technical Note No. 902, National Advisory Committee for Aeronautics, Washington, D.C., USA, 1943.

[26] J. Lubliner, *Plasticity Theory*, Dover Publications, New York, NY, USA, 2008.

[27] J. Simo and T. Hughes, "Objective integration algorithms for rate formulations of elastoplasticity," *Computational Inelasticity, Interdisciplinary Applied Mathematics*, vol. 7, pp. 276–299, 1998.

[28] K. Johnson, W. Karunasena, N. Sivakugan, and A. Guazzo, "Modeling pile-soil interaction using contact surfaces," in *Computational Mechanics–New Frontiers for the New Millennium*, S. Valliappan and N. Khalili, Eds., pp. 375–380, Elsevier, Amsterdam, Netherlands, 2001.

[29] D. Sheng, K. D. Eigenbrod, and P. Wriggers, "Finite element analysis of pile installation using large-slip frictional contact," *Computers and Geotechnics*, vol. 32, no. 1, pp. 17–26, 2005.

[30] N. Strömblad, "Modeling of soil and structure interaction subsea," Master's Degree Thesis, Chalmers University, Sweden, 2014.

[31] M. Hassanein, M. Elchalakani, A. Karrech, V. Patel, and E. Daher, "Finite element modelling of concrete-filled double-skin short compression members with CHS outer and SHS inner tubes," *Marine Structures*, vol. 61, pp. 85–99, 2018.

[32] L. Arany, S. Bhattacharya, J. Macdonald, and S. Hogan, "Design of monopiles for offshore wind turbines in 10 steps," *Soil Dynamics and Earthquake Engineering*, vol. 92, pp. 126–152, 2017.

[33] Abs, *ABS Rules for Building and Classing- Steel Vessels 2008*, American Bureau of Shipping (ABS), Houston, TX, USA, 2008.

[34] G. L. Dnv, "Standard dnvgl-st-0437: loads and site conditions for wind turbines," Technical Report, DNV GL: Oslo, Norway, 2016.

[35] E. J. Laya, J. J. Connor, and S. S. Sunder, "Hydrodynamic forces on flexible offshore structures," *Journal of Engineering Mechanics*, vol. 110, no. 3, pp. 433–448, 1984.

[36] Applied Technology Council, *Quantification of Building Seismic Performance Factors, FEMA P695*, Applied

Technology Council, Federal Emergency Management Agency, Washington, DC, USA, 2009.

[37] A. S. Veletsos, "Dynamics of structure-foundation systems," in *Structural and Geotechnical Mechanics*, W. J. Hall, Ed., pp. 333–361, Prentice-Hall, Englewood Cliffs, NJ, USA, 1977.

[38] G. Gazetas, "Formulas and charts for impedances of surface and embedded foundations," *Journal of Geotechnical Engineering*, vol. 117, no. 9, pp. 1363–1381, 1991.

[39] D. Lombardi, S. Bhattacharya, and D. Muir Wood, "Dynamic soil–structure interaction of monopile supported wind turbines in cohesive soil," *Soil Dynamics and Earthquake Engineering*, vol. 49, pp. 165–180, 2013.